International Journal of Applied Engineering Research ISSN 0973-4562 Volume 12, Number 5 (2017) pp. 656-663

Effects of Features of Graphite Nodules on Stress Concentration in Nodular Graphite Cast Iron Material under Multi-Axial Loading

Adnan D. Mohammed[1] and Mahmoud Kachit[2]

[1]Mechanical engineering Department, Faculty of Engineering, Philadelphia University, Amman, Jordan.

[2] Mechanical engineering Department, Faculty of Engineering, Mutah University, Karak, Jordan.

Abstract

This research is concerned with the determining of best configuration features of graphite nodules, (spherical or elliptical in shape), embedded in cast iron matrix, that contribute in reducing the stress concentration. Experimental and numerical studies were carried out to satisfy the aims. Results show that the plane of stress concentration and thusly the critical planes of cracking and propagation are perpendicular to the loading axis. X-Ray tomography demonstrated that cracks appear to take the path of high-density nodules. The stress concentration increments as the nodule size increments, yet this tendency is clearer when the size is smallest. The effect of the intensity of applied stress on the came about stress concentration is profoundly noticed in the case of large size nodules. The stress concentration increases rapidly as the inter-distance displays little values. The stress concentration decreases as the dimension ratio of the elliptical nodule increases. It has minimum value when the ellipse long dimension is aligned with the axis of applied stress. However, it is maximum when the orientation angle is about 90°.

Keywords: Nodular cast Iron, spherical graphite nodules, elliptical graphite nodules, stress concentration, multi-axial loading.

INTRODUCTION

Various elements supporting the initiation of micro-cracks are reported in the literature. We note, in the first place, the unique characteristics of crack initiating defects, that is to say, their size and shape, and their environment, such as inter-nodule distance or the default position relative to the surface the specimen.

Understanding the microstructural mechanisms of crack initiation and propagation, as well as knowledge associated to quantitative data are needed for two reasons. On the one hand, it allows establishing and developing reliable models for calculating the real strength limit. This theme will not be discussed here. On the other hand, understanding the cracking mechanisms as function of defects site, morphology and distribution allows considering optimization solutions vis-à-vis of mechanical strength limit. It is this second point that concerns us in this study. We will therefore pay particular attention to the influence of microstructure on GS fonts on cracking mechanisms.

PREVIOUS STUDIES

In nodular cast irons the graphite nodules and micro-shrinkage cavities, which is inherently present, lead to a reduction in ultimate strength limit [1]. Crack initiation is affected by the following factors:

Nature of crack initiating sites: Three possible modes boot fatigue cracks are reported in the literature: Out of the matrix along slip bands from defects; debonding of the interface inclusion/matrix and rupture of inclusion. In the case of spheroidal graphite cast iron, crack initiation is generally observed on two types of faults: the graphite nodules and porosities comprising shrinkage and microshrinkage.

The first crack initiating site concerns with micro-cracking phenomena that occur around certain graphite nodules. In the field ($\sigma_{app} = \sigma_{0,2}$), crack initiation is done with the equator of the graphite nodules perpendicular to the loading direction [2, 3, 4, 5, and 6]. At stronger stress ($\sigma_{app} > \sigma_{0,2}$), Dierickx [7] has shown that de-coherence phenomena at the poles nodule intervened.

The second crack initiating site is at the level of porosity zones [8, 9, and 10]. There are sometimes, in certain cast iron alloys, other crack initiating sites as those mentioned above. Thus, in the case of GS perlito - ferritic cast irons, micro-cracks can initiate at the border between the pearlite and ferrite [10], however, this case is still rare.

Features of crack initiating sites: Various factors favoring the initiation of microcracks are reported in the literature. We note first the unique characteristics of crack initiating defects, that is to say, their size and shape, and their environment, such as nodule inter-distance or the default position relative to the surface the specimen.

P.A.S. Reed *et al.* [11] and Ravichandran *et al*. [12] have compared the characteristics of initiating and noted crack initiating defects in ADI cast stressed in four point bending. They have observed that the diameter of the nodule initiating microcracks is approximately greater by a factor 2. However, the diameter of graphite nodules in principle remains less than 100 microns.

From a theoretical point of view, previous studies, (using FE analysis), reference [13] has shown that Von Mises stress was maximum in the equatorial plan of defect. This result can explain why nucleation of microcrack occurs at the defect equator but not occurs on the bigger defects. As a matter of fact, 3D micro-tomographic observations showed that the bigger defect size, the less spherical shape and the less smooth the surface.

In nodular cast iron, it is known that the pure torsional strength is insensitive to small defects or notches [14]. The critical size of a non-detrimental defect increases with increase in the combined stress ratio. It appears that nodules and cavities can act harmfully to lower the fatigue strength under all combinations of normal and shear stresses. The shape of the defect also appears to have an influence. Palin-Luc T. *et al.* [3] have noticed, in a melting GS perlito-ferritic that initiation of microcracks occurs around very irregularly shaped graphite nodules. Moreover, it is well known that local stresses are minimal with a spherical geometry and increase with another geometry [15].

Observations of GS perlito-ferritic cast iron have shown that when the distance between the nodules is low, the initiation of micro-cracks is favored [3].

Location relative to the surface

Verdu [16] has noted that the size of the surface area of the graphite nodules initiating microcracks is smaller than the size of those that do not initiating. This is explained by the fact that the nodule having a small surface, have however a large size below the surface. This author observes the presence of the non-propagating cracks, which are initiated on nodule located below the surface. In this study, as against, the nature of defects is different because they were basically micro-shrinkage [10]. In nodular cast irons, micro-cracks were observed at the equator of the casting defects (microshrinkage) and graphite nodules [16]. X-ray tomography confirmed that microcracks were nucleated only on defects located at or near the sample surface (distance between the defect and the surface lower than 10µm). No microcrack was observed in the bulk. The probability of a defect to initiate a crack was correlated with the size of the defect but also with its location with respect to the surface sample. The maximum fraction of initiated defect was obtained for $0.75< Dd /Wd<1$, where Wd is the Defect size measured on the surface, and Dd is the defect depth under the surface. Moreover, the most critical defects were the biggest located just under the sample surface. Finite Element analysis [17] concluded that in the case of spherical cavities, strain localization occurred in the ligament of material between the cavity and the free surface. This strain localization was most severe for cavities just touching the surface.

Endo [14] has shown, for FCD700 and FCD400 nodular cast iron and 0.37% carbon steel, that a defect can become most harmful when it is located just below the free surface, and the greater the defect is in size, the more detrimental it will be to the mechanical strength.

Regarding crack propagations, the cracks form, initially inside the ligament of matrix between the surface and the defect, whatever the type of defect (spheroid or porosity) [18]. The ratio Ls/Wd, (Ls is the crack length on the specimen's surface and Wd is the defect size measured on the surface), remained less than one. Moreover for the defects which are just touched the surface, this ratio could be very small. It suggests that any crack did not propagate beyond the defect as already observed [16].

EXPERIMENTAL INVESTIGATIONS

Tensile tests were conducted at MATEIS laboratory - INSA Lyon - France. The tests were carried out using servo-controlled hydraulic testing machine (see Figure 1). Crack orientation was investigated after the rupture of specimens using Optical Microscope (OM) and Scanning Electronic Microscope (SEM). The test specimens were made of spherical graphite ferritic cast iron (GS). The material was chemically characterized, and the chemical composition is displayed in Table 1.

Table 1: Chemical composition (% mass) of the tested material

C	*Si*	*Mn*	*S*	*P*	*Mg*
3.4	2.60	0.19	0.005	0.011	0.05

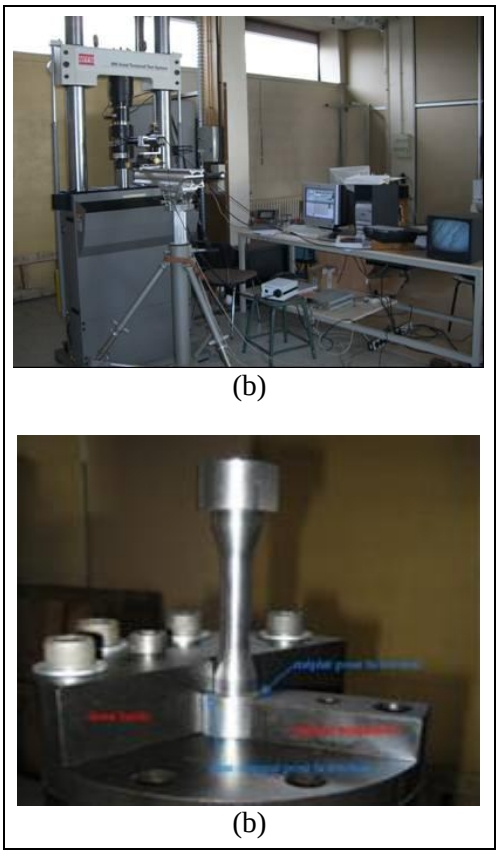

(b)

(b)

Figure 1: Experimental set-up

Mechanical properties were obtained using monotonic tensile tests. The averaged (over two tests) properties are shown in table 2. The elastic modulus was obtained by the method of

resonance frequency of a bar made of the material mentioned above.

The specimens are cylindrical in shape having a gage length of 25 mm, and a diameter of 6mm (Figure 2). Polishing has been done longitudinally on the gage length to obtain a flat narrow band (0.5×7mm) which is allowing a good OM and SEM observation of cracks.The monotonic tests, at strain rate of 1mm/min, were conducted at room temperature until rupture. The crack initiation, propagation and orientation in the matrix and at the graphite nodules were studied as function of features of graphite nodule using OM and SEM after rupture of specimens.

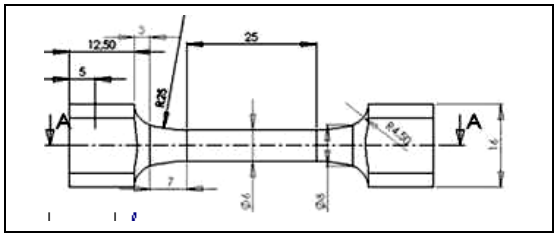

Figure 2: Geometry of tested specimens

Table 2: Mechanical properties of the tested material

E (GPa)	$\sigma_{0.2}$ (MPa)	σ_r (MPa)	A%
168	270	400	20

NUMIRICAL INVESTIGATIONS

A finite element model comprises of graphite nodule embedded in a cylindrical iron bar (matrix). The bar is fixed at one end and free at the other end, as shown in Figure 3. This model was built up and analyzed using Ansys-15 software. A controlled axial loading was applied to the model. The latter contains graphite nodule(s) of different features. The effect of graphite nodule morphology (size, nodule inter-distance, a/b ellipse ratio and ellipse orientation angle) on the concentration of Von Mises stress was investigated. The fixed end of the model (cylinder) was made like a horn in shape to prevent undesirable stress concentration that may occur at sharp edges.

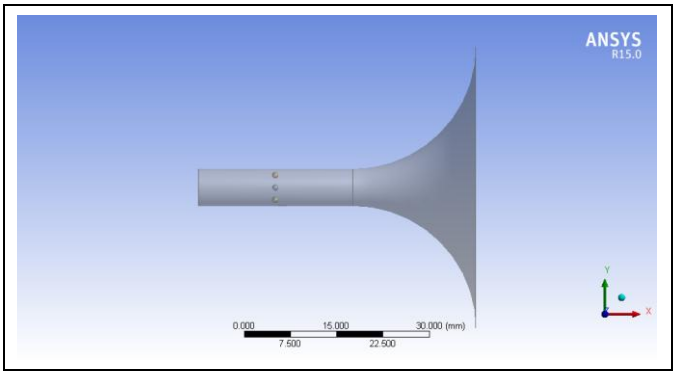

Figure 3: Finite Elements model

EXPERIMENTAL RESULTS

Crack orientation, initiation and propagation were studied after rupture of the specimens. Figure 4 demonstrates the behavior of some non-propagating cracks and micro-cracks in the matrix and in graphite nodule. In this figure, it can be seen that all micro-cracks are initiated and propagated, in general, perpendicularly (i.e., 0° between the normal crack plan and specimen axis). Consequently, the specimens were broken at perpendicular plans to specimen axis, and the fracture surface is quite plan without tortuosity (Figure 4.a). All micro-cracks are perpendicular to the specimens axis and they can initiate both at the interface matrix/nodules (at the equator of graphite nodules) (Figure 4.b and Figure 4.d). They are rarely occurring in the matrix (Figure 4.c). Some cracks contour the nodules and separate it from the matrix (Figure 4.d).

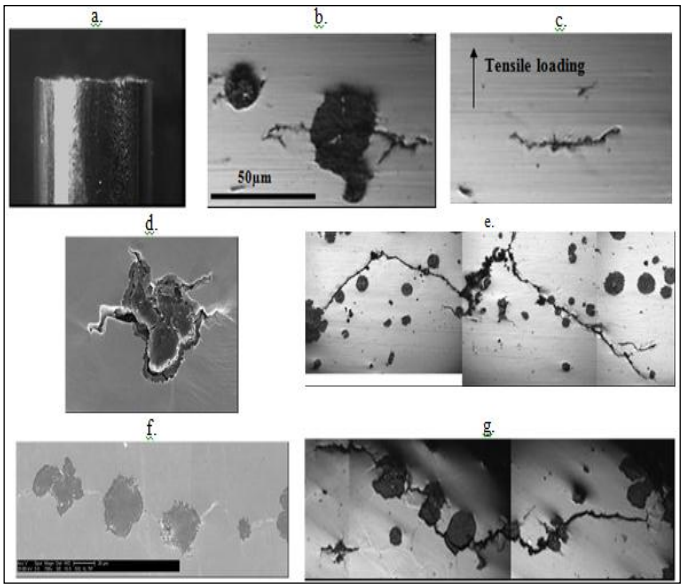

Figure 4: (a) Broken specimen, (b – g) Cracks at the interface matrix/nodules (at the equator of graphite nodules) and in the matrix

The proportion of cracks initiated in the matrix is very low. It is about 20% and 30% of total cracks for the two tested specimens respectively. The rarely observed matrix cracks were not accompanied with local plastic zone and it seems that they initiate due to nodules situated just below the surface (Figure 4.c). The cracks form initially inside the ligament of matrix between the surface and the defect whatever the type of defect (spheroid or porosity). Once the microcracks initiate at nodules they can propagate perpendicularly in the matrix. Cracks coalescence between nodules can be observed in Figure 4.e, Figure 4.f, and Figure 4.g.

Not all graphite nodules can initiate micro-cracks (with stresses below the strength limit) because the conditions for initiation are not met for all nodules. In this study, only 10% (for the two tested specimens) of the nodules initiate propagating microcracks. Once these micro-cracks are initiated, two scenarios are possible; they will propagate (in some cases) and eventually cause rupture of the specimen or, (in other cases), these microcracks will remain blocked by the microstructure

features and there will be no propagation leading to failure. 3D pictures of X-ray tomography for some cracks were done to explain the behavior of cracks inside the material. The small number of studied cracks does not allow an exact conclusion on the cracking behavior in volume. Qualitatively, during their propagation inside the material, the cracks seem to take the path of high-density nodules, but they, in general propagate inside the material in a direction that is perpendicular to the specimen axis (Figure 5).

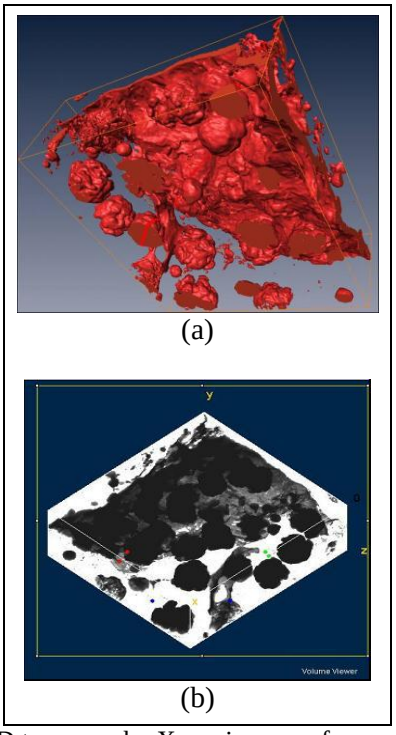

Figure 5: 3D tomography X-ray images of a crack at the end of fatigue life

NUMERICAL RESULTS

The effects of applied stress and nodule size:

A controlled axial loading was applied along the longitudinal axis of the FE model (cylinder). The embedded graphite nodule was modeled, first, as a sphere (Figure 6). Different sizes (diameters) of graphite nodules were considered (between 50 and 1000µm). As it can be seen, the Von Mises stresses concentrate as a ring around the nodule, in a plan that is perpendicular to the direction of the applied stress. Consequently, it can be expected that the crack initiates as a ring around the nodule, and perpendicular to the applied stress direction.

It was found that there is a good agreement between results obtained from both experimental (see Figure 4b) and numerical studies (Figure 6). The plane of stress concentration and consequently the critical planes of cracking are perpendicular to the loading axis.

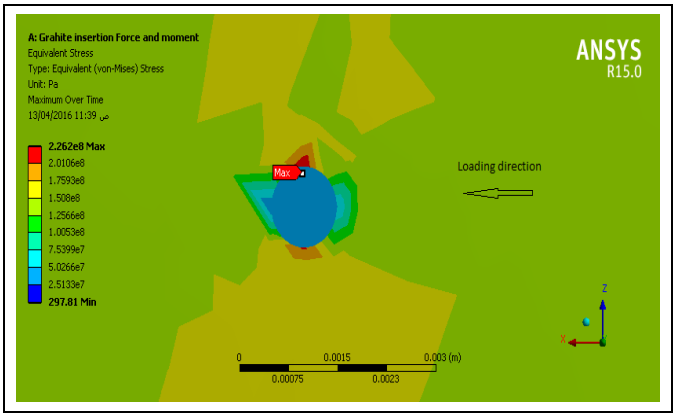

Figure 6: Critical plan is perpendicular to the model's longitudinal axis

The effects of nodule size and the applied stress on the resulted concentration of maximum Von Mises stress are shown in Figure 7. Stress concentration increases as the applied stress and nodule size increase. The concentration reaches, approximately, 125% of the applied stress for the smallest size of nodule (50µm) under an applied stress of 125MPa. It reaches, approximately, 425% of the applied stress for the largest of nodule size (1000µm) under an applied stress of 175Mpa. This figure demonstrates that stress concentration increases, in linear fashion, as the applied stress increases.

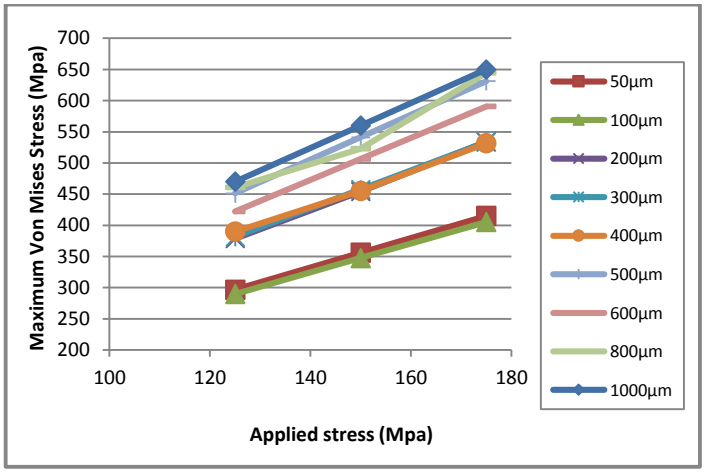

Figure 7: Von-Mises stress as function of applied stress for different nodule sizes

This figure allows tracing the sensitivity of Von Mises stress to applied stress, (normalized Von Mises stress), by considering the slope of curves shown in Figure 8. The sensitivity increases linearly with the nodule size. It changes from 2.3 for the smallest nodule size to 3.7 for the largest nodule size.

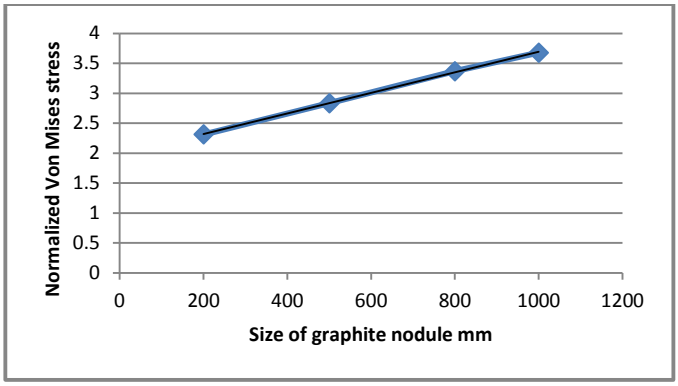

Figure 8: Sensitivity of Von Mises stress to applied stress for different nodule's size

Figure 7 also allows to obtain the sensitivity of Von Mises stress to nodule size (the evolution of Von Mises stress relative to the evolution of nodule size) as shown in Figures 9 and 10. The sensitivity increases linearly with the size of nodule. This sensitivity is highly noticed in the domain of 50-300 µm than that shown in the domain 300-1000 µm. Sensitivity mean value is about 4MPa/µm, for low nodule size, and 0.15MPa/µm, for high nodule size.

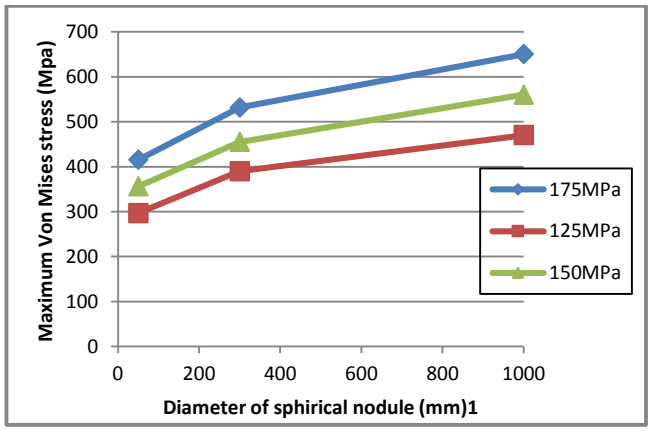

Figure 9: Von Mises stress as function of nodule's size for different applied stress amplitudes

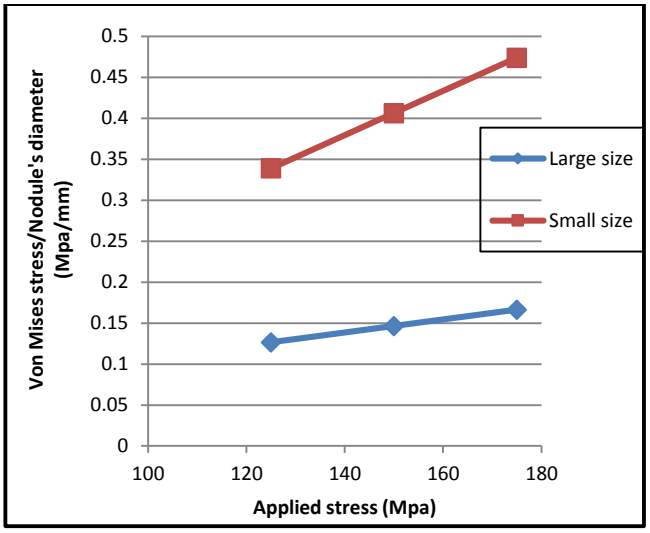

Figure10: Sensitivity of Von Mises stress to nodule size for different applied stress amplitudes

The effect of nodules inter-distance (center to center distance):

The effect of nodule inter-distance (center to center distance of two adjacent spheres) was investigated on models having embedded nodules of size of 50µm and for the three applied stress values, (125, 150 and 175MPa). The maximum Von Mises stress concentration between two adjacent spheres do not touch each other when the inter distance is high, as demonstrated in Figure 11.a. The maximum concentration keeps having the profile of a ring around the surface of the sphere. When the inter distance is low, Von Mises stress concentrates at the interconnection of the two adjacent spheres.

A good agreement is noticed between numerical results (Figure 11b) and experimental results (Figure 4g), that critical plan are perpendicular to model's axis.

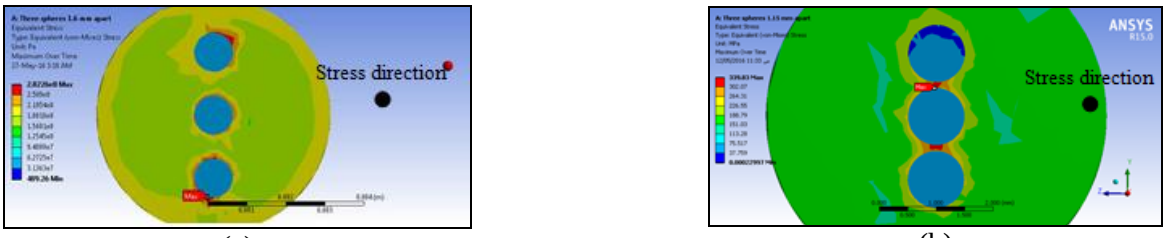

(a) (b)

Figure 11: The concentration of Von Mises stress at the connecting zone between the nodules. (a) large inter-distance, (b) small inter-distance

The effect of nodules inter-distance and applied stress on stress concentration is shown in Figure 12. Stress concentration increases as the applied stress increases and as nodule inter-distance decreases. The stress concentration reaches approximately 350% of the applied stress for the lowest value of nodule inter-distance (1.01 mm), and 125% of the applied stress value for the highest value of nodule inter-distance (1.25 mm). As shown in the figure, the concentration of stress increases linearly as the applied stresses increases. This figure allows tracing the sensitivity of Von Mises stress to applied

stress for the selected values of inter-distance as shown in figure 13.

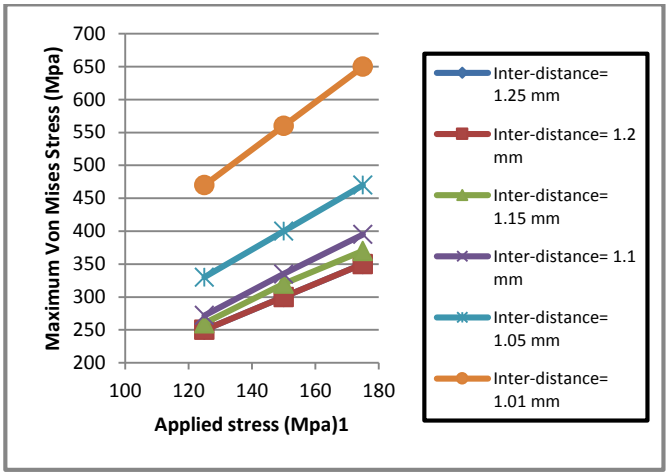

Figure 12: Von Mises stress as function of applied stress for different values nodule's inter-distance

This sensitivity (normalized Von Mises stress) increases, (following a polynomial function of third order), as the nodule inter-distance decreases. It varies from the value of 2 for the largest nodule inter-distance, to the value of 3.7 for the smallest inter-distance.

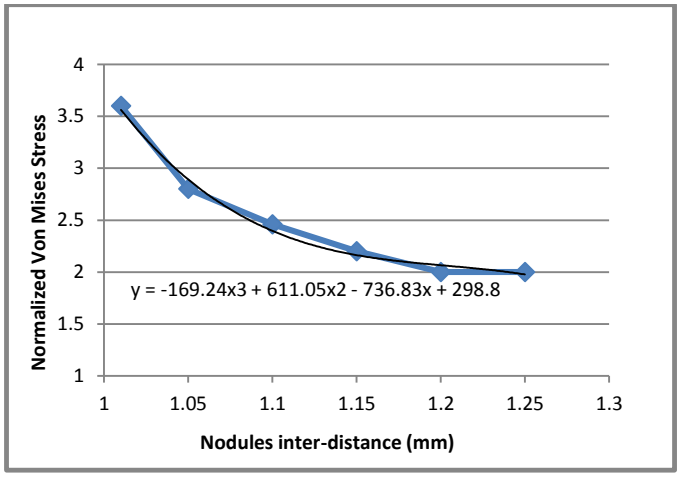

Figure 13: Sensitivity of Von Mises stress to applied stress for different nodule inter-distances

The demonstrated results may lead to micro-crack initiation in the interconnection zone between the two adjacent nodules.

The effect of dimensions ratio (a/b) of the elliptical nodule:

The effect of features of nodules having the shape of an ellipse was also investigated numerically. The governing parameter in this investigation was the ellipse ratio a/b, where "a" is the ellipse dimension along the direction of the applied stress (x-axis) and "b" is the other dimension of the ellipse (along y-axis). The stress concentration was monitored at the surface facing the applied stress (Figure 14).

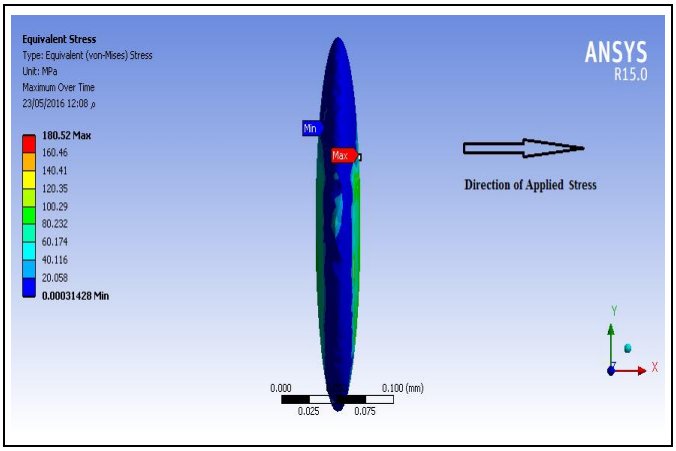

Figure 14: The concentration of Von Mises stress on an elliptical graphit

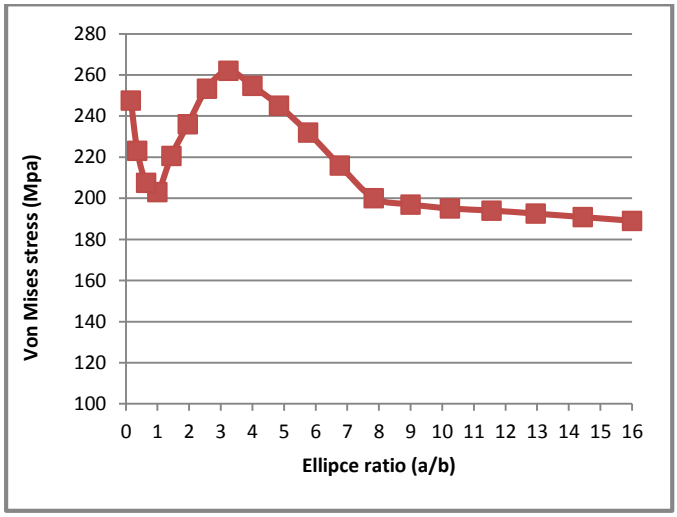

Figure 15: Von Mises stress in function of ellipse ratio (a/b)

Results of stress concentration due to applied axial loading are shown in Figure 15. The stress concentration is minimum when a/b=1. It increases as a/b approaches 0 and for 1< a/b < 4. For a/b > 4, the stress concentration decreases sharply until the ratio a/b approaches the value of approximately 8, then it decreases slowly, and reach a minimum value for a/b value of 16.

The effect of orientation angle of elliptical nodule

The effect of ellipse orientation angle with the model's longitudinal axis (axis of applied stress) was also investigated for the ratio a/b=10. The orientation angle was varied from 0° to 180° (ellipse is aligned horizontally) passing by 90° (ellipse is aligned vertically). Typical picture of orientation is shown in figure 16 for an angle of 45° and a/b ratio of about 10.

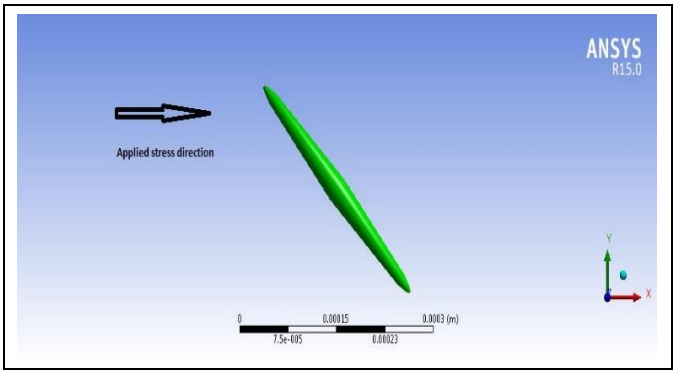

Figure 16: Elliptical graphite nodule at 45 degrees orientation angle, a= 160 μm, b=15.625 μm .

Figure 17 displays the variation of stress concentration with the orientation angle. It shows a symmetric behavior around the value of angle of 90°. The stress concentration is highest when the angle is 90° and minimum at 0° and 180°.

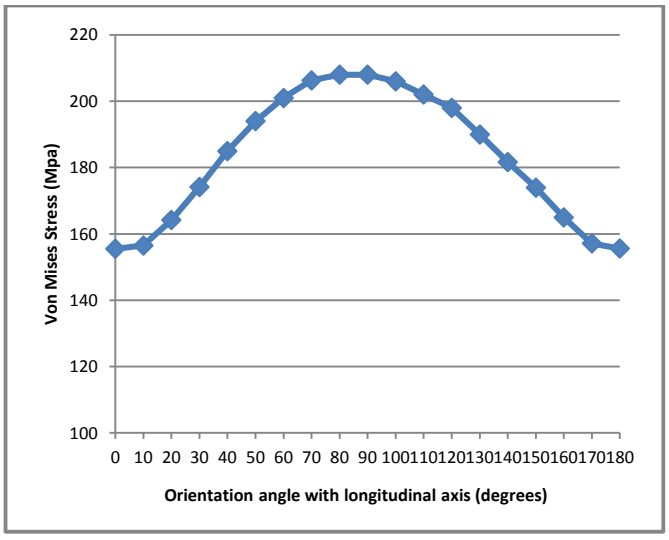

Figure 17: The variation of stress concentration with ellipse orientation angle

CONCLUSIONS

Experimental and numerical studies were carried out to determine the best configuration features of graphite nodules, (spherical or elliptical in shape), embedded in cast iron matrix, that contribute in reducing the stress concentration**.** It is found that stress concentration increases as the nodule size increases. This tendency is more important when the size is within the low size domain of value [50-300 μm]. Three dimension images of X-ray tomography showed cracks that seem to take the path of high-density nodules, but they propagate inside the material (generally) in a direction that is perpendicular to the model's longitudinal axis. The applied stress has a noticeable effect on increasing stress concentration for the cases when the sizes of the nodules are relatively large. For the case of elliptical graphite nodule, it is found that stress concentration decreases as the ellipse ratio (a/b) of the elliptical nodule increases. Moreover, the orientation angle (with the axis of loading) of elliptical nodule has the highest influence, (maximum stress concentration), when the angle is close to 90°. This research recommended that nodular graphite cast iron should be prepared, fabricated and heat treated to obtain the optimal features leading to minimum values of stress concentration. The size of the embedded nodule has to be the smallest possible for spherical nodules and largest possible for the case of elliptical embedded nodules. The elliptical nodule is better to be aligned with axis of the applied external stress in order to produce minimum stress concentration.

ACKNOWLEDGEMENT

The authors greatly acknowledge the supports given by the Faculty of Engineering and the Faculty of Scientific Research and Higher Education at Philadelphia University, Amman, Jordan.

REFERENCES

[1] Marquis G.B. and Karjalainen-Roikonen, P. ,2003, "Long-life multiaxial fatigue of a nodular graphite cast iron". Andrea Carpinteri, Manuel de Freitas and Andrea Spagnoli, *"Biaxial/Multiaxial Fatigue and Fracture*". Elsevier , New York, pp 105-122.

[2] Monchoux, J. P. ,2000, "Influence of the ferritizing annealing on the microstructure and cracking mechanisms in monotonic and cyclic loadings of the perlito-ferritic spheroidal graphite cast iron", Ph. D. thesis in Materials Engineering. National Institute of Applied Sciences in Lyon, France. (In French).

[3] Palin-luc, T., Lasserre, S., Berard, 1998, "Experimental investigation on the significance of the conventional endurance limit of a spheroidal graphite cast iron", Journal of fatigue & fracture of Engineering Materials & Structures, 21, pp 191-200.

[4] Clement, P. , Angeli, J.P., Pineau, A., 1984, "Short crack behavior in nodular cast iron", Journal of Fatigue & fracture of Engineering Materials & Structures, 7, pp. 251-265.

[5] Nadot, Y., 1997, "Influence of casting defects on the fatigue strength of a ductile iron", Ph. D. thesis. University of Poitier. France. (in French)

[6] Suzuki, A., Hirose, Y., Yajima, Z., Tanaka, K., 1993, "Fatigue crack nucleation and growth behavior of ductile cast iron", International Journal of Fatigue, 27, pp. 9-21. (in Japanese).

[7] Dierickx, P., 1996, "Study of the microstructure and damage mechanisms in GS ductile irons: influence of heat treatment ferritisation", Ph. D. thesis in Materials Engineering. National Institute of Applied Sciences, Lyon, France. (In French).

[8] Nadot, Y., J. Mendez, J., Ranganathan et al., 1999, "Fatigue life assessment of nodular cast iron containing casting defects", Journal of Fatigue & fracture of Engineering Materials & Structures", 22, pp. 289-300.

[9] Tokaji, K., Ogawa, T., 1996, "Fatigue life distribution and its simulation in spheroidal graphite cast irons", Materials Science Research International, 2, pp. 39-45.

[10] Nadot, Y., 1997, "Influence of casting defects on the fatigue strength of a ductile iron ', Ph. D. thesis in Materials Science. National School of Mechanical and Aeronautical Engineering, Poitier, France. (In French).

[11] Reed, P. A. S., Thomson, R. C., J.S. James, J. C. , Putman, D. C., Lee, K. K., Gunn, S. R., 2003, "Modeling of microstructural effects in the fatigue of austempered ductile iron", Materials Science and Engineering *(A)*, 346: 1-2, pp. 273-286.

[12] K.S. Ravichandran, K. S., R. Ritchie, R. O., Murakami, Y., 1999, "Small Fatigue Cracks: Mechanics, Mechanisms and Applications". Elsevier, New York.

[13] Bentachfine, S., Pluvinage, G., 1996, "Biaxial low cycle fatigue under non-proportional loading of a magnesium-lithium alloy", Engineering fracture mechanics, 54 pp. 513-522.

[14] Endo, M., 2003, "The multiaxial fatigue strength of specimens containing small defects". Andrea Carpinteri, Manuel de Freitas and Andrea Spagnoli, *Biaxial/Multiaxial Fatigue and Fracture*, Elsevier, New York, pp. 243-264.

[15] Kang, G., Gao, Q., Yang, X., 2004, "Uniaxial and non-proportionally multiaxial ratcheting of SS304 stainless steel at room temperature: experiments and simulations", International Journal of Non-Linear Mechanics, 39, pp. 843 – 857.

[16] Verdu, C, Adrien, J., Buffière, J. Y., 2008, "Three-dimensional shape of the early stages of fatigue cracks nucleated in nodular cast iron", Materials Science and Engineering (A); 483–484, pp. 402–405.

[17] Xiaoshan, L., Guoqiu, H., Xiangqun, D., Defeng, M., Weihua, Z., 2009, "Fatigue behavior and dislocation substructures for 6063 aluminum alloy under non proportional loadings", International Journal of Fatigue, 31, pp. 1190-1195.

[18] Endo, M., Ishimoto, I., 2006, "The fatigue strength of steels containing small holes under out-of-phase combined loading", International Journal of Fatigue, 28, pp. 592–597.